THE JOURNAL OF PHYSICAL CHEMISTRY LETTERS
A JOURNAL OF THE AMERICAN CHEMICAL SOCIETY

pubs.acs.org/JPCL

Letter

Wall-Confined Spreading Dynamics on the Surface of Surfactant Solution

Wenjie Ji, Ding Lan,* Weibin Li, Quanzi Yuan,* and Yuren Wang

Cite This: *J. Phys. Chem. Lett.* 2022, 13, 4315−4320

Read Online

ACCESS | Metrics & More | Article Recommendations | Supporting Information

ABSTRACT: A liquid spreading over another is a universal physical process in the nature, which was investigated by the scaling law to reveal the underlying mechanical mechanism over the decades. However, scaling laws are restricted to piecewise physical stages, respectively. It is a challenge to present a full physical picture for a dynamic spreading process covering a wide-spectrum speed. We propose a general wall-confined spreading dynamics (WCSD) model originating from molecular kinetic theory (MKT). It creatively illustrates the order and domination between driving energy and energy dissipation (or transfer) using a phase diagram according to theory and experiments. This work reveals the deep mechanical mechanism of WCSD which provides an indirect guidance on the solution processing methods of two-dimensional molecular crystals (2DMCs) growth.

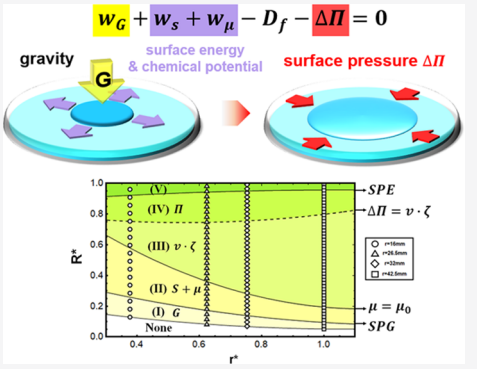

Since Benjamin Franklin's wave-stilling experiment on water, oil spreading on the aqueous surface has attracted extensive attention. Recently, there has been renewed interest in wetting or spreading phenomena involving an ordered pattern,[1−4] Marangoni flow,[5] droplet evaporation[6−9] and bouncing[10,11] as well as applications in the gas cavity,[12] biological droplet rectifiers,[13] alignment of a 2D nanosheet,[14] thin-film synthesis in flexible electronics,[15] and 2DMCs growth.[16−18] A large number of investigations about spreading dynamics have indicated that a spreading process is self-similar and scale-invariant, where its scaling law (e.g., spreading radius $R \sim t^{\alpha}$) can effectively reveal the mechanical mechanism in the view of hydrodynamics and MKT.[19]

The scaling law in hydrodynamics is established by mechanical balance and boundary conditions with viscous dissipation.[20] For spreading on deep liquid support, the boundary layer approximation applies with typical power laws including gravity-inertial ($R \sim t^{1/2}$), gravity-viscous ($R \sim t^{1/4}$), and surface tension-viscous regimes ($R \sim t^{3/4}$).[21,22] Among them, ($R \sim t^{3/4}$) is the most common one which has been verified several times in experiments.[23−25] High-Reynolds-number flow occurs, and there is viscous dissipation within the viscous boundary layer.[26] For spreading on thin support, the lubrication approximation applies. The fixed bottom surface restricts the flow and low-Reynolds-number viscous flow occurs in the entire support[27] with $R \sim t^{1/2}$ for Marangoni-viscous spreading.[28] In addition, the scaling law also depends on the spatial distribution dimension of spreading substances. The surface tension-viscous balance on thin support leads to $R \sim t^{1/2}$ for a front (1D),[28] $R \sim t^{1/3}$ for a planar strip (2D),[29] and $R \sim t^{1/4}$ for an axisymmetric droplet (3D).[30] In the same way, a similar conclusion $R(t) \sim t^{3/2(n+2)}$ for deep support can be obtained:[31] $R \sim t^{3/4}$ ($n = 0$) for constant-concentration line source (1D);[24] $R \sim t^{1/2}$ ($n = 1$) for strip with fixed mass (2D);[25] $R \sim t^{3/8}$ for axisymmetric droplet (3D).[26] Moreover, a series of scaling laws can be derived for complex interfacial topology (e.g., the spreading of oil by condensed water drops with $R \sim t^{1/2}$ for constant thickness, $R \sim t^{1/4}$ for constant volume, and $R \sim t^{1/6}$ for thin film flow).[43] The power law is relevant to the concentration boundary condition at the origin as well.[5,29]

MKT is a statistical physical method originating from absolute rate theory, which establishes the connection between molecular motion and macroscopic flow.[32] It emphasizes molecular-scale friction dissipation near the contact line rather than viscous dissipation in the bulk.[33] Gravity-viscous spreading for 3D follows $R \sim t^{1/8}$[34] and $R \sim t^{1/10}$ for 3D capillary-viscous regime (Tanner's law),[35] while $R \sim t^{1/7}$ for capillary-friction regime (3D) in MKT[36−38] as well as $R \sim t^{1/5}$ (2D).[32]

However, a general physical model to match the spreading process with a wide-spectrum speed is still lacking,[37] and physical significance is not clear sometimes due to the coupling of multiple interactions. In this paper, we propose a general physical model that unifies and connects these discrete stages

Received: March 31, 2022
Accepted: May 4, 2022
Published: May 9, 2022

https://doi.org/10.1021/acs.jpclett.2c00928
J. Phys. Chem. Lett. 2022, 13, 4315−4320

instead of conventional piecewise scaling laws. WCSD process is recognized combining theories and experiments. We propose divisional phase diagram of WCSD to illustrate corresponding physical significance. This work reveals the deep mechanical mechanism of WCSD with indirect applications in solution processing method of 2DMCs growth involving in solution epitaxy,[18] space-confined self-assembly,[17] layer-defined solution self-assembly strategy,[16] etc.

First, we are going to discuss the theoretical model of an oil droplet spreading dynamics on surfactant aqueous surface in a confined vessel. In the view of MKT, the speed of moving contact line (MCL) v depends on the difference between forward κ^+ and backward fluctuating frequencies κ^- of oil molecular displacements from one adsorption site to another. The equation of MCL dynamics can be expressed as[39]

$$v = \lambda(\kappa^+ - \kappa^-) = 2\kappa^0\lambda \sinh\left(\frac{w}{2nk_BT}\right) \tag{1}$$

where w is driving work, κ^0 equilibrium frequency, k_B the Boltzmann constant, T absolute temperature, λ jump length, and n adsorption sites number ($n\lambda^2 = 1$).

In classical thermodynamics, the Helmholtz free energy F includes the following forms of energy transfer in an isotherm surface system ($dT = 0$),

$$dF = \gamma_i\, dA_i + \mu_k\, dN_k \tag{2}$$

where γ the interface energy, A the interface area, μ the chemical potential, and N the number of particles entering the system. The gravity potential φ and the pair of surface stress−strain (σ^s_{ij},ε^s_{ij}) are introduced into the system with its free energy per unit area

$$\left.\frac{dF}{dA}\right|_{T,V} = \varphi + \mu_k\frac{dN_k}{dA} + \frac{\sigma_{ij}{}^s d\varepsilon_{ij}{}^s}{dA/A} \tag{3}$$

where gravity potential φ works for a capillary-scale droplet spreading. Equation 3 is the surface Gibbs−Duhem equation specialized for the surfactant system in this paper. The surface strain energy density $\frac{\sigma_{ij}{}^s d\varepsilon_{ij}{}^s}{dA/A}$ can be expressed by surface energy using $\frac{\sigma_{ij}{}^s d\varepsilon_{ij}{}^s}{dA/A} = S = S_i - \Delta\Pi$, where S, S_i, and Π represent the final, initial spreading coefficient, and surface pressure, respectively.

Hence, the driving work w in MKT comes from three contributions corresponding to eq 3, including gravity potential, chemical potential, and surface energy (spreading coefficient). First, the driving work of the gravity potential can be expressed as[40]

$$w_G = \varphi = \frac{1}{2}\rho g e^2 \tag{4}$$

where e is the thickness of the spreading oil. The initial spreading coefficient

$$w_s = S_i = \gamma_{wv} - \gamma_{ov} - \gamma_{ow} \tag{5}$$

drives spreading initially, where γ_{wv}, γ_{ov}, and γ_{ow} represent the water-vapor, oil-vapor, and oil-water interface energies, respectively. With the increasing amount of oil molecules transferring from its bulk phase into interfacial layer, it is worth noting that chemical potential $\Delta\mu$ is another driving work that should be considered and $\Delta\mu$ keeps accumulating with spreading until it reaches maximum μ_0 (when $t > \tau$, $\Delta\mu \approx \mu_0$),

$$w_\mu = \Delta\mu = \mu_k\frac{dN_k}{dA} = \mu_0(1 - e^{-t/\tau}) \tag{6}$$

where τ is the characteristic time of molecular diffusion. Here the ratio of driving work $w = w_G + w_\mu + w_s$ to thermal energy k_BT is of the order of 0.01−0.1 ($w \sim \sinh(w/(2nk_BT))$); therefore, eq 1 can be simplified to

$$w - v\cdot\zeta = 0, \left(v \approx \frac{w}{\zeta}\right) \tag{7}$$

where $\zeta = \frac{k_BT}{\kappa^0\lambda^3}$ represents the friction coefficient per unit length. Equation 7 is established by the balance between driving work w and energy dissipation $D_f = v\cdot\zeta$ at the molecular scale.

Besides, it should be noticed that some of the system energy would be converted into surface pressure Π (also known as surface elastic energy) due to the compressed surfactant monolayer in a confined area.[41] The surface pressure Π of adsorbed surfactant pushes outward along the air−solution interface, acting to increase the surface area.[42] Based on the Volmer isotherm model, considering finite molecule size lateral interactions, the increment in surface pressure follows[42]

$$\Delta\Pi = \frac{k_BT\Gamma}{1 - \Gamma/\Gamma_\infty} - \frac{k_BT\Gamma_0}{1 - \Gamma_0/\Gamma_\infty} \tag{8}$$

where $\Gamma = N/\pi(r^2 - R^2)$ the surface excess concentration; N number of surfactant molecules on the water surface; r the inner radius of container; R the spreading radius (defined by nominal contact line on the observation scale). After taking these factors into account, eq 7 can be modified to

$$w_G + w_s + w_\mu - D_f - \Delta\Pi = 0 \tag{9}$$

After every item is substituted into eq 9, it becomes

$$\frac{1}{2}\rho g\left(\frac{V_0^2}{\pi^2R^4}\right) + S_i + \mu_0(1 - e^{-t/\tau}) - v\cdot\zeta - \left(\frac{k_BT\Gamma}{1 - \Gamma/\Gamma_\infty} - \frac{k_BT\Gamma_0}{1 - \Gamma_0/\Gamma_\infty}\right) = 0 \tag{10}$$

Equations 9 and 10 are established by the balance between driving work $w = w_G + w_s + w_\mu$ and friction dissipation D_f at the molecular scale as well as surface pressure $\Delta\Pi$.

According to eq 9, spreading dynamics here can be considered as the coupling and linear superposition of several effects including gravity, surface energy, chemical potential, friction dissipation, and surface pressure, etc. We are going to evaluate each factor separately next. The initial spreading stage should be driven by gravity because body force dominates the spreading near the capillary scale as shown in Figure 1a, where surfactants molecules are sparsely distributed on the aqueous surface in Figure 1d. In the next stage, uneven distribution of the spreading substance on the aqueous surface leads to a surface tension gradient and the growth of chemical potential with a thinner oil layer (thickness ≪ capillary scale) as shown in Figure 1b but retarded by surface pressure in the end in Figure1c. The surface pressure is generated by the compressed surfactant monolayer ahead of the nominal contact line during spreading in a confined vessel as shown in Figure 1e. As a result, kinetic energy transfers into surface elastic energy, and

https://doi.org/10.1021/acs.jpclett.2c00928
J. Phys. Chem. Lett. 2022, 13, 4315−4320

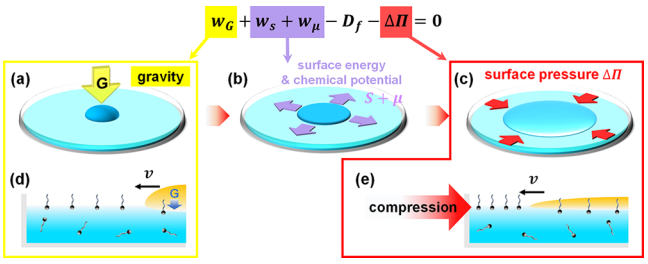

Figure 1. Several possible forces in different stages and the corresponding state of surfactant monolayer in a spreading process: the spreading driven by gravity (a) and the sparse distribution of surfactant molecules on an aqueous surface (d); the spreading driven by surface energy and chemical potential along the aqueous surface (b); the spreading retarded by surface pressure leading to an quasi-equilibrium state (c) and the dense distribution of surfactant monolayer on a compressed aqueous surface (e).

spreading is balanced by the surface pressure ΔΠ. As the spreading rates decays, the friction-elasticity transition may occur.

A general spreading experiment is carried out, and 9 μL of *n*-hexadecane droplet is deposited on the surface of sodium dodecyl sulfate (SDS) aqueous solution (depth of 2.5 mm). Here we investigated quasi-equilibrium states for different aqueous solution concentrations including 0.5, 1, 1.5, and 2 times the critical micelle concentration (CMC) in different-sized vessels. The schematic diagram of the experimental setup is shown in Figure 2a. It is observed that the maximum

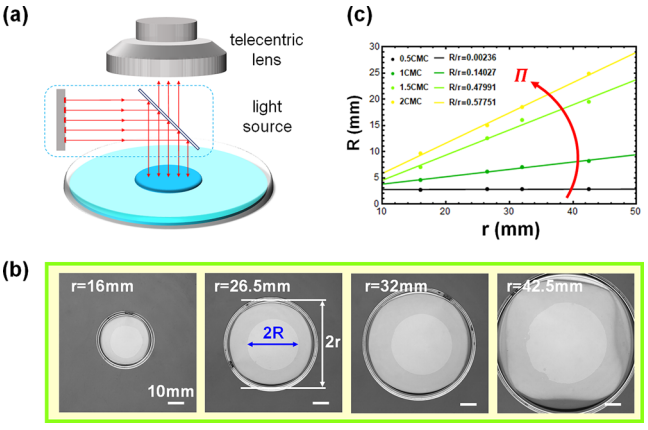

Figure 2. (a) Schematic representation of the experimental setup composed of telecentric lens and coaxial lighting source. (b) Top view of maximum spreading area of 9 μL of *n*-hexadecane droplet on SDS solution (2CMC) in different-sized vessels. (c) Relation between maximum spreading radius R and vessel radius r in different concentrations of base solution (including 0.5CMC, 1CMC, 1.5CMC, 2CMC).

spreading radius is proportional to the vessel radius as shown in Figure 2b,c. According to the generalized isotherm of a monolayer, its state follows $\Pi = k_B T\Gamma$ (Henry model).[42] It leads to $R/r = \sqrt{1 - \Pi_0/\Pi}$ (see S1 in the Supporting Information for details) which is consistent with every experimental group that the data points are linearly distributed along the fitting lines at a concentration from 0.5CMC to 2CMC as shown in Figure 2c. The slope R/r of fitting line relates to the surface pressure or surface excess. According to the slope R/r of the fitting line in Figure 2c, it comes a conclusion that there is a higher surface pressure at a higher solution concentration. Therefore, both the quasi-equilibrium state and spreading dynamic process depend on the surface pressure as well as the state of the surfactant monolayer.

However, driving energy, energy transfer, and dissipation are usually coupled with each other in a WCSD. Here, a valid manner is proposed to decouple them by combing fitting and numerical solution. The fitting curve of the numerical solution of eq 10 matches well with experimental result (2CMC) of spreading radius over time in Figure 3a where the parameters are selected as follows: r = 42.5 mm, ζ = 0.27 Pa s, S_i = 2.6 mN/m, $\mu_0 = 1.7 \times 10^{-3}$ J/mol, $\Gamma_0 = 8.782 \times 10^{-7}$ mol/m^2 (see S2 in the Supporting Information for details). It can be observed that a general spreading usually involves several stages of accelerating first, then decelerating, and balancing in Figure 3a. In order to reveal the physical mechanism in each stage, we have considered each term in eq 9 separately in numerical method. When the gravity term w_g is ignored, the fitting curve deviates from the experimental results at the first three data points in the yellow block in Figure 3b, but it is still consistent with other experimental data. The separation point of gravity (SPG) occurs almost in the same time scale (~40 ms) for the spreading in different-sized vessels. It illustrates that gravity only works in the initial stage and has nothing to do with the size of the vessels (see S3 in the Supporting Information for details). When the surface pressure ΔΠ in eq 9 is ignored, the fitting curve will detach from the experimental results from the separation point of elasticity (SPE) in the green block and oil would continue to spread far beyond its quasi-equilibrium state as the red curve shows in Figure 3c (see similar results for other-sized vessels in S4 of the Supporting Information for details). It indicates that the surface compressive elasticity will dominate the resistance from SPE.

Though the physical mechanism is partially revealed above, there is still strong coupling. So what are the order and magnitude of the driving energy, friction dissipation, as well as surface elasticity in an entire spreading process? In further exploration, we divide these dynamic spreading processes into several areas in a normalized phase diagram (Figure 3d) to illustrate corresponding physical significance clearly. The initial radius of the droplet before spreading is almost the same for every group, as the line shows at the starting point in Figure 3d. Considering the gravity effect, the area below the line of SPG can be considered as a gravity area marked as (I) in Figure 3d. With the droplet collapsing and thinning, the surface tension gradient dominates and the chemical potential gradually accumulates until saturation as expressed in eq 10. The area between the line of saturation points and SPG is the chemical potential (and surface tension) area marked as (II). For the spreading processes after stage (II), the driving energy keeps almost constant so that the resistance becomes the main factor for spreading. The surfactant monolayer on the aqueous surface is continuously compressed with oil spreading so that surface pressure replaces friction dissipation gradually. Comparing the friction dissipation and surface elasticity, the dashed line in Figure 3d representing the equality of the two ($\Delta\Pi = v{\cdot}\zeta$) is taken as the reference for the area division. The area below the dashed line can be considered as the friction dissipation area marked as (III), while the area above it is dominated by surface elasticity marked as (IV). The top area above SPE marked as (V) in Figure 3d represents a quasi-equilibrium state with a constant surface pressure correspond-

https://doi.org/10.1021/acs.jpclett.2c00928
J. Phys. Chem. Lett. 2022, 13, 4315−4320

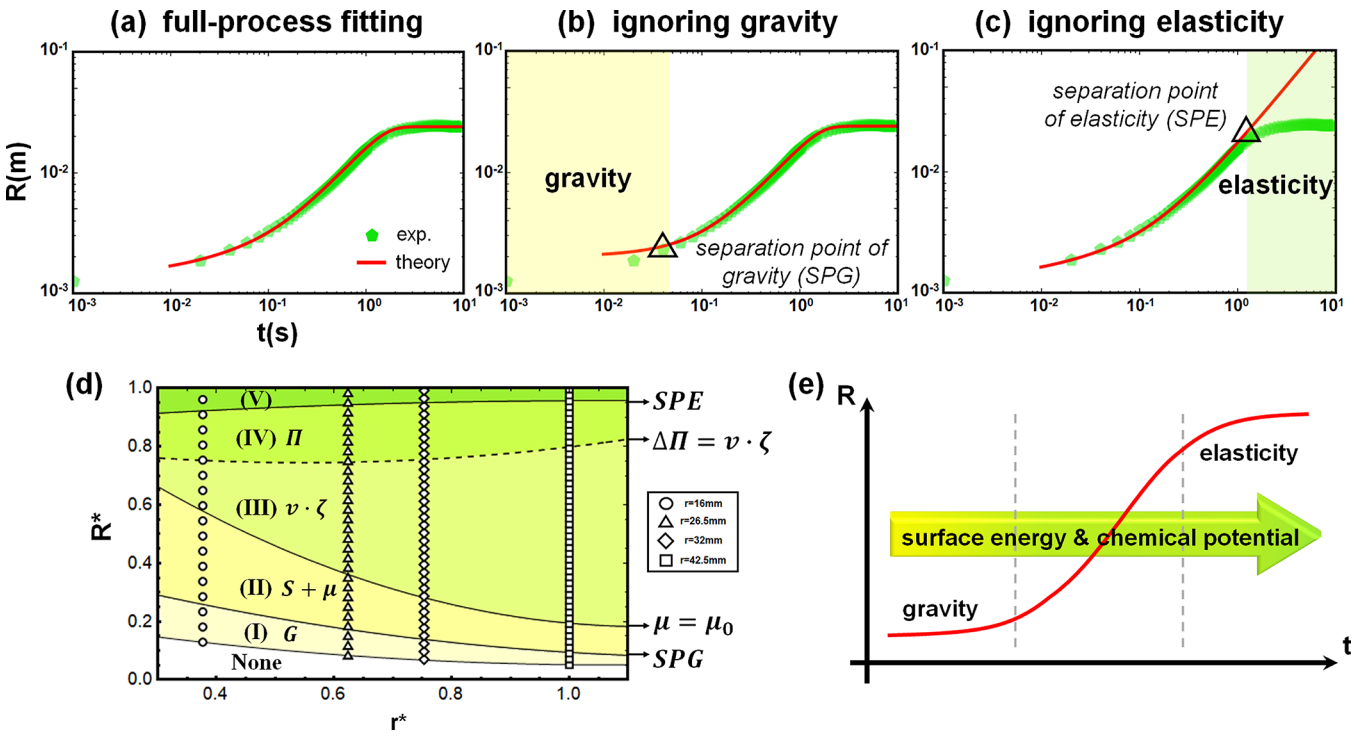

Figure 3. Experimental data is represented by green pentagons where R is the spreading radius of the droplet in 42.5 mm-radius vessel. (a) The full-process fitting curve (in red) originating from a numerical solution in eq 10. (b) The fitting ignoring gravity with a yellow block corresponding to the gravity region (from the initial point to the separation point of gravity (SPG)). (c) The fitting ignoring surface elasticity with a light green block corresponding to the elasticity region (from the separation point of elasticity (SPE) to the end). (d) The phase diagram illustrating the physical process of spreading in different-sized vessels with corresponding partitions (where $r^* = r/r_{max}$, $R^* = R/R_{max}$). (e) The physical picture of a spreading process on the surfactant aqueous surface.

ing to a green block in Figure 3c. (See more details about the basis of classification in S5 of the Supporting Information.)

Here, we divide the spreading process into several stages from (I) to (V) with corresponding physical significance. In stages (I) and (II), gravity, surface energy, and chemical potential account for a higher proportion in a smaller vessel as shown in Figure 3d. On the contrary, pure friction dissipation (after chemical potential reaches saturated) in stage (III) accounts for a larger proportion in larger vessels. However, it is almost the same proportion for the surface elasticity in stages (IV) and (V) in different vessels. It indicates that surface elasticity dominates resistance when the surfactant monolayer ahead of the contact line is compressed to the same relative variation ($R^* \approx 0.8$ in Figure 3d) with the same surface pressure, which coincides with the linear "R−r" relation of the quasi-equilibrium state in Figure 2c. The friction-elasticity transition is found in the end of wall-confined spreading.

Hence, the spreading process can be separated into three stages: gravity effect in the initial stage, surface energy and chemical potential effect in the intermediate stage, and wall-confined effect (surface elasticity) in the quasi-equilibrium stage as shown in Figure 3e. It is worth noting that chemical potential and surface energy play a major role not only in the intermediate stage but in the entire spreading. When the chemical potential is not considered, the fitted curve is no longer reasonable and is far from the experimental results, even for the case without considering the surface energy S_i (see S6 in the Supporting Information for details). In addition, this model is able to be simplified to derive a series of scaling laws as follows. For a pancake-shaped droplet, gravity and friction dominate the spreading in the initial stage with $R \sim t^{1/5}$. As the droplet spreads, chemical potential replaces gravity gradually to balance the friction with $R \sim t$. Specifically, for a spherical-cap-shaped droplet, capillarity-friction dominates in the initial stage leading to $R \sim t^{1/7}$. The power exponent α derived from the WCSD model ($1/7 < \alpha < 1$) involves most of the current main conclusions (see S7 in the Supporting Information for details).

In summary, a full physical picture of WCSD is revealed, which unifies the discrete physical stages instead of the conventional scaling law. A general confined spreading can be separated into three stages: gravity stage, intermediate stage, and quasi-equilibrium stage. Gravity participates in the initial stage of spreading, and then surface tension and chemical potential play an important role instead of gravity. In the vicinity of the quasi-equilibrium stage, friction-elasticity transition occurs and surface elasticity dominates. The time scale of gravity action is independent of the vessel size in experiments. According to numerical solutions, there is a larger pure friction proportion in larger vessel, but the surface elasticity acts in almost the same proportion for different vessel sizes leading to the linear "R−r" relation. Therefore, the spreading area and dynamic process can be tuned by selecting the vessel size. This model is able to derive a series of scaling laws which satisfies most of the previous conclusions. In addition, the conclusion in this paper is not only limited to the surfactant system but also applicable to other aqueous solution systems satisfying the adsorption isotherms model. This work brings about a deeper understanding to the mechanical mechanism of WCSD and also provides an indirect guidance on how to create an ideal circumstance for the solution processing method of 2DMCs growth by tuning physical property parameters.

https://doi.org/10.1021/acs.jpclett.2c00928
J. Phys. Chem. Lett. 2022, 13, 4315−4320

■ ASSOCIATED CONTENT

Supporting Information

The Supporting Information is available free of charge at https://pubs.acs.org/doi/10.1021/acs.jpclett.2c00928.

Details about quasi-equilibrium state (section S1); several fitting results (sections S2−S4, S6); basis of classification in phase diagram (section S5); and several scaling laws derived from the WCSD model (section S7) (PDF)

■ AUTHOR INFORMATION

Corresponding Authors

Ding Lan − *National Microgravity Laboratory, Institute of Mechanics, Chinese Academy of Sciences, Beijing 100190, People's Republic of China;* orcid.org/0000-0001-9688-7731; Email: landing@imech.ac.cn

Quanzi Yuan − *State Key Laboratory of Nonlinear Mechanics, Institute of Mechanics, Chinese Academy of Sciences, Beijing 100190, People's Republic of China; School of Engineering Sciences, University of Chinese Academy of Sciences, Beijing 100049, People's Republic of China;* orcid.org/0000-0003-4255-6181; Email: yuanquanzi@lnm.imech.ac.cn

Authors

Wenjie Ji − *National Microgravity Laboratory, Institute of Mechanics, Chinese Academy of Sciences, Beijing 100190, People's Republic of China; School of Engineering Sciences, University of Chinese Academy of Sciences, Beijing 100049, People's Republic of China;* orcid.org/0000-0002-6560-0731

Weibin Li − *National Microgravity Laboratory, Institute of Mechanics, Chinese Academy of Sciences, Beijing 100190, People's Republic of China;* orcid.org/0000-0002-6406-1553

Yuren Wang − *National Microgravity Laboratory, Institute of Mechanics, Chinese Academy of Sciences, Beijing 100190, People's Republic of China*

Complete contact information is available at: https://pubs.acs.org/10.1021/acs.jpclett.2c00928

Notes

The authors declare no competing financial interest.

■ ACKNOWLEDGMENTS

This work was jointly supported by the Strategic Priority Research Program of Chinese Academy of Sciences (Grant Nos. XDA17030100, Y820081XD1, and Y820082XD1) and the National Natural Science Foundation of China (Grant No. 12072346)

■ REFERENCES

(1) Mouat, A. P.; Wood, C. E.; Pye, J. E.; Burton, J. C. Tuning Contact Line Dynamics and Deposition Patterns in Volatile Liquid Mixtures. *Phys. Rev. Lett.* **2020**, *124* (6), 064502.

(2) Yamamoto, D.; Nakajima, C.; Shioi, A.; Krafft, M. P.; Yoshikawa, K. The Evolution of Spatial Ordering of Oil Drops Fast Spreading on a Water Surface. *Nat. Commun.* **2015**, *6*, 7189.

(3) Wodlei, F.; Sebilleau, J.; Magnaudet, J.; Pimienta, V. Marangoni-Driven Flower-like Patterning of an Evaporating Drop Spreading on a Liquid Substrate. *Nat. Commun.* **2018**, *9*, 820.

(4) Keiser, L.; Bense, H.; Colinet, P.; Bico, J.; Reyssat, E. Marangoni Bursting: Evaporation-Induced Emulsification of Binary Mixtures on a Liquid Layer. *Phys. Rev. Lett.* **2017**, *118* (7), 074504.

(5) Roche, M.; Li, Z.; Griffiths, I. M.; Le Roux, S.; Cantat, I.; Saint-Jalmes, A.; Stone, H. A. Marangoni Flow of Soluble Amphiphiles. *Phys. Rev. Lett.* **2014**, *112* (20), 208302.

(6) Man, X.; Doi, M. Vapor-Induced Motion of Liquid Droplets on an Inert Substrate. *Phys. Rev. Lett.* **2017**, *119* (4), 044502.

(7) Man, X.; Doi, M. Ring to Mountain Transition in Deposition Pattern of Drying Droplets. *Phys. Rev. Lett.* **2016**, *116* (6), 066101.

(8) Wu, M.; Doi, M.; Man, X. The Contact Angle of an Evaporating Droplet of a Binary Solution on a Super Wetting Surface. *Soft Matter.* **2021**, *17* (34), 7932−7939.

(9) Wu, M.; Di, Y.; Man, X.; Doi, M. Drying Droplets with Soluble Surfactant. *Langmuir* **2019**, *35* (45), 14734−14741.

(10) Hao, C.; Li, J.; Liu, Y.; Zhou, X.; Liu, Y.; Liu, R.; Che, L.; Zhou, W.; Sun, D.; Li, L.; Xu, L.; Wang, Z. Superhydrophobic-Like Tunable Droplet Bouncing on Slippery Liquid Interfaces. *Nat. Commun.* **2015**, *6*, 7986.

(11) Qian, C.; Zhou, F.; Wang, T.; Li, Q.; Hu, D.; Chen, X.; Wang, Z. Pancake Jumping of Sessile Droplets. *Adv. Sci.* **2022**, *9* (7), 2103834.

(12) Zhu, S.; Wu, T.; Bian, Y.; Chen, C.; Zhang, Y.; Li, J.; Wu, D.; Hu, Y.; Chu, J.; Li, E.; Wang, Z. Sustaining Robust Cavities with Slippery Liquid-Liquid Interfaces. *Adv. Sci.* **2022**, *9* (7), 2103568.

(13) Li, J.; Li, J.; Sun, J.; Feng, S.; Wang, Z. Biological and Engineered Topological Droplet Rectifiers. *Adv. Mater.* **2019**, *31* (14), 1806501.

(14) Zhao, C.; Zhang, P.; Zhou, J.; Qi, S.; Yamauchi, Y.; Shi, R.; Fang, R.; Ishida, Y.; Wang, S.; Tomsia, A. P.; Liu, M.; Jiang, L. Layered Nanocomposites by Shear-Flow Induced Alignment of Nanosheet. *Nature.* **2020**, *580* (7802), 210−215.

(15) Yuan, K.; Song, T.; Yang, C.; Guo, J.; Sun, Q.; Zou, Y.; Jiao, F.; Li, L.; Zhang, X.; Dong, H.; Li, L.; Hu, W. Polymer-Assisted Space-Confined Strategy for the Foot-Scale Synthesis of Flexible Metal−Organic Framework-Based Composite Films. *J. Am. Chem. Soc.* **2021**, *143* (42), 17526−17534.

(16) Yao, J.; Zhang, Y.; Tian, X.; Zhang, X.; Zhao, H.; Zhang, X.; Jie, J.; Wang, X.; Li, R.; Hu, W. Layer-Defining Strategy to Grow Two-Dimensional Molecular Crystals on a Liquid Surface down to the Monolayer Limit. *Angew. Chem., Int. Ed.* **2019**, *58* (45), 16082−16086.

(17) Wang, Q.; Yang, F.; Zhang, Y.; Chen, M.; Zhang, X.; Lei, S.; Li, R.; Hu, W. Space-Confined Strategy toward Large-Area Two-Dimensional Single Crystals of Molecular Materials. *J. Am. Chem. Soc.* **2018**, *140* (16), 5339−5342.

(18) Xu, C.; He, P.; Liu, J.; Cui, A.; Dong, H.; Zhen, Y.; Chen, W.; Hu, W. A General Method for Growing Two-Dimensional Crystals of Organic Semiconductors by "Solution-Epitaxy. *Angew. Chem., Int. Ed.* **2016**, *55* (33), 9519−9523.

(19) Bonn, D.; Eggers, J.; Indekeu, J.; Meunier, J.; Rolley, E. Wetting and Spreading. *Rev. Mod. Phys.* **2009**, *81* (2), 739−805.

(20) Dandekar, R.; Pant, A.; Puthenveettil, B. A. Film Spreading from a Miscible Drop on a Deep Liquid Layer. *J. Fluid Mech.* **2017**, *829*, 304−327.

(21) Hoult, D. P. Oil Spreading on the Sea. *Annu. Rev. Fluid Mech.* **1972**, *4*, 341−368.

(22) Hoult, D. P. *Oil on the Sea*; Plenum: New York, 1969.

(23) Bergeron, V.; Langevin, D. Monolayer Spreading of Polydimethylsiloxane Oil on Surfactant Solutions. *Phys. Rev. Lett.* **1996**, *76* (17), 3152−3155.

(24) Foda, M.; Cox, R. G. The Spreading of Thin Liquid Films on a Water-Air Interface. *J. Fluid Mech.* **1980**, *101* (1), 33−51.

(25) Dussaud, A. D.; Troian, S. M. Dynamics of Spontaneous Spreading with Evaporation on a Deep Fluid Layer. *Phys. Fluids.* **1998**, *10* (1), 23−38.

(26) Jensen, O. E. The Spreading of Insoluble Surfactant at the Free Surface of a Deep Fluid Layer. *J. Fluid Mech.* **1995**, *293*, 349−378.

(27) Gaver, D. P.; Grotberg, J. B. The Dynamics of a Localized Surfactant on a Thin Film. *J. Fluid Mech.* **1990**, *213*, 127−148.

(28) Borgas, M. S.; Grotberg, J. B. Monolayer Flow on a Thin Film. *J. Fluid Mech.* **1988**, *193*, 151−170.

(29) Jensen, O. E.; Grotberg, J. B. Insoluble Surfactant Spreading on a Thin Viscous Film: Shock Evolution and Film Rupture. *J. Fluid Mech.* **1992**, *240*, 259−288.
(30) Dussaud, A. D.; Matar, O. K.; Troian, S. M. Spreading Characteristics of an Insoluble Surfactant Film on a Thin Liquid Layer: Comparison between Theory and Experiment. *J. Fluid Mech.* **2005**, *544*, 23−51.
(31) Berg, S. Marangoni-Driven Spreading along Liquid-Liquid Interfaces. *Phys. Fluids* **2009**, *21* (3), 032105.
(32) Blake, T. D.; Haynes, J. M. Kinetics of Liquid/Liquid Displacement. *J. Colloid Interface Sci.* **1969**, *30* (3), 421−423.
(33) Ralston, J.; Popescu, M.; Sedev, R. Dynamics of Wetting from an Experimental Point of View. *Annu. Rev. Mater. Res.* **2008**, *38*, 23−43.
(34) Cazabat, A. M.; Stuart, M. A. C. Dynamics of Wetting: Effects of Surface Roughness. *J. Phys. Chem.* **1986**, *90* (22), 5845−5849.
(35) Tanner, L. H. The Spreading of Silicone Oil Drops on Horizontal Surfaces. *J. Phys. D: Appl. Phys.* **1979**, *12* (9), 1473−1484.
(36) Ehrhard, P.; Davis, S. H. Non-Isothermal Spreading of Liquid Drops on Horizontal Plates. *J. Fluid Mech.* **1991**, *229*, 365−388.
(37) Ren, W.; Hu, D.; E, W. Continuum Models for the Contact Line Problem. *Phys. Fluids* **2010**, *22* (10), 102103.
(38) Yuan, Q.; Zhao, Y. Precursor Film in Dynamic Wetting, Electrowetting, and Electro-Elasto-Capillarity. *Phys. Rev. Lett.* **2010**, *104* (24), 246101.
(39) Blake, T. D.; De Coninck, J. The Influence of Solid-Liquid Interactions on Dynamic Wetting. *Adv. Colloid Interface Sci.* **2002**, *96* (1−3), 21−36.
(40) de Gennes, P.-G; Brochard-Wyart, F.; Quéré, D. *Capillarity and Wetting Phenomena: Drops, Bubbles, Pearls, Waves*; Springer: New York, 2003.
(41) Langevin, D. Rheology of Adsorbed Surfactant Monolayers at Fluid Surfaces. *Annu. Rev. Fluid Mech.* **2014**, *46*, 47−65.
(42) Manikantan, H.; Squires, T. M. Surfactant Dynamics: Hidden Variables Controlling Fluid Flows. *J. Fluid Mech.* **2020**, *892*, 1 DOI: 10.1017/jfm.2020.170.
(43) Chaudhury, M. K.; Chaudhury, A. Super Spreading of Oil by Condensed Water Drops. *Soft Matter.* **2005**, *1* (6), 431−435.

https://doi.org/10.1021/acs.jpclett.2c00928
J. Phys. Chem. Lett. 2022, 13, 4315−4320